Full paper

Metallocene implanted metalloporphyrin organic framework for highly selective CO_2 electroreduction

Zhifeng Xin [a,b,1], Yi-Rong Wang [a,1], Yifa Chen [a,**], Wen-Liang Li [c], Long-Zhang Dong [a], Ya-Qian Lan [a,*]

[a] Jiangsu Collaborative Innovation Centre of Biomedical Functional Materials, Jiangsu Key Laboratory of New Power Batteries, School of Chemistry and Materials Science, Nanjing Normal University, Nanjing, 210023, PR China
[b] Institute of Molecular Engineering and Applied Chemistry, Anhui University of Technology, Ma'anshan, Anhui, 243002, PR China
[c] Faculty of Chemistry, Northeast Normal University, Changchun, 130024, PR China

ARTICLE INFO

ABSTRACT

Metal organic frameworks (MOFs) with tunable porosity and metal sites have been considered as excellent candidates for electrochemical CO_2 reduction reaction (CO_2RR). However, the poor electron conductivity and electron-donating capability of MOFs constrain the improvement of catalytic efficiency. Herein, we implant metallocene in MOFs through a facile chemical vapor deposition method and thus-obtained catalysts present excellent CO_2RR electrocatalysis performances. For instance, the FE_{CO} of $CoCp_2$@MOF-545-Co can be as high as 97% at −0.7 V. The high performances might be attributed to the strong binding-interaction between metallocene and metalloporphyrin that can largely reduce the adsorption energy of CO_2 as revealed by density functional theory calculations. The introduction of metallocene can serve as electron donor and carrier to create continuous electron transfer channel in MOFs and provide strong binding-interaction with metalloporphyrin during CO_2RR process to enhance the CO_2RR activity. This method might shed light on development of highly-selective CO_2RR electrocatalysts.

1. Introduction

The excessive emission of carbon dioxide (CO_2) has arisen to be a serious environmental problem in the world [1]. Diverse techniques have been proposed to efficiently store or convert CO_2 [2]. Concerning the economy and energy consumption, the conversion of carbon dioxide into fuels or other useful chemicals is considered as the most promising approach to solve the problem [3]. Electrocatalytic CO_2 reduction reaction (CO_2RR) as a kind of controllable, environmental-friendly and high efficiency approach has been regarded as one of the most powerful way to transform CO_2 into serviceable high-valued energy products (e. g., CO, CH_4, HCOOH and C_2H_5OH, etc.) and might simultaneously mitigate the green-house effect or energy crisis [4–8]. However, it is still hard to meet the demand of practical applications and the exploration of efficient CO_2RR electrocatalysts is highly desirable.

In recent years, many researchers have focused on the exploration of catalysts for electrocatalytic CO_2RR [9–11] and diverse materials such as metals [12,13], transition metal oxides [14], transition metal chalcogenides [15], metal-free 2D materials [16–18] and metal-organic frameworks (MOFs) [19–21] have been developed. There are some basic principles for the design of target CO_2RR electrocatalysts: 1) active catalysis sites; 2) high selectivity and 3) efficient electron transfer channel, etc. However, despite the interesting and intriguing field in exploring fantastic materials, obstacles like low selectivity, instability and complicated processes in material fabrication have largely impaired the development of electrocatalytic CO_2RR.
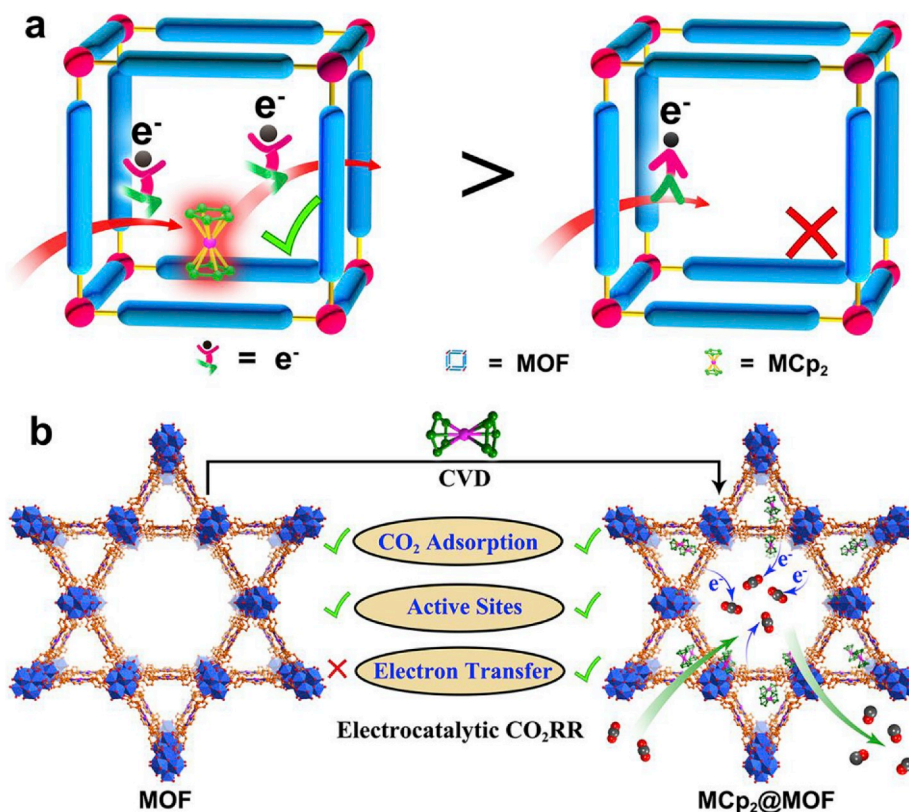
MOFs, assembling from inorganic metal ions or clusters and organic ligands have been regarded as ideal platforms for electrocatalytic CO_2RR [22–25]. The tunable porosity and functional metal sites imparting MOFs with favorable capability for CO_2 adsorbing and efficient catalysis centers might create catalytic environments suitable for CO_2RR [26,27]. Yet, the poor electrical conductivity and electron donating capability set obstacles for MOFs being as efficient CO_2RR electrocatalysts, concerning the necessary multiple electron transfer processes for achieving any

---

* Corresponding author.
** Corresponding author.
E-mail addresses: chyf927821@163.com (Y. Chen), yqlan@njnu.edu.cn (Y.-Q. Lan).
[1] The two authors are equally contributed.

Fig. 1. The schematic presentation for the advantages of MCp$_2$@MOF in electrocatalytic CO$_2$RR. (a) The schematic presentation of introducing MCp$_2$ in MOF structure to improve the electron transfer ability for electrocatalyticCO$_2$RR. (b) The comparison of MCp$_2$@MOF and MOF in electrocatalytic CO$_2$RR.

highly-selective products. To conquer it, diverse strategies have been proposed and can be mainly divided into two categories: in-situ growth of novel MOF structures and integration of multi-functional units in MOF based composites. For in-situ growth, MOFs such as ZIF-8, HKUST-1, Al$_2$(OH)$_2$-TCPP-Co and Re-SURMOF have been investigated for the generation of diverse CO$_2$RR products like CO, CH$_4$, HCOOH or C$_2$H$_4$, etc [28–30]. However, the poor electrical conductivity or insufficient electron donating capability impairs most of MOFs to be efficient electrocatalysts, resulting in low selectivity unmet for practical applications. Some pioneering reports have integrated electron-rich units (e. g., [PMo$_8^V$Mo$_4^{VI}$O$_{35}$Zn$_4$] cluster) into MOFs to largely improve the selectivity of CO$_2$RR [29]. However, it is still challenging to select proper ligands and electron-rich units to construct novel MOFs with high selectivity and efficiency. Despite the in-situ growth of MOFs, integration of multi-functional units (e.g., nanoparticles) in MOFs with the advantages like ease of processing, versatile in material selection and potential in generation of highly selective products is another promising method to achieve efficient MOF based CO$_2$RR electrocatalysts. For example, the introducing of functional units like copper nanoparticle or 1,10-phenanthroline can increase the selectivity of MOFs to generate HCOOH or CO [31,32]. However, the selection of desired materials or MOFs and the exploration of powerful methods to integrate multi-functionality in MOFs for the efficient generation of high-valued products are still challenging and long-sought-after.

Therefore, the strategy is highly important to construct novel MOF based materials with target functionalities like numerous active sites or continuous electron transfer channels to facilitate the process of electrocatalytic CO$_2$RR. Metallocene (MCp$_2$, Cp stands for cyclopentadienyl) is an electron-rich system with high stability and aromaticity [33]. In MCp$_2$ electron orbits, the participation of d-orbits enlarges the π-electron system of cyclopentadienyl ring, thus making MCp$_2$ to be perfect electron-donating or carrying unit. When the metallocene is implanted into the structure of MOFs, MCp$_2$ can serve as potential electron donator
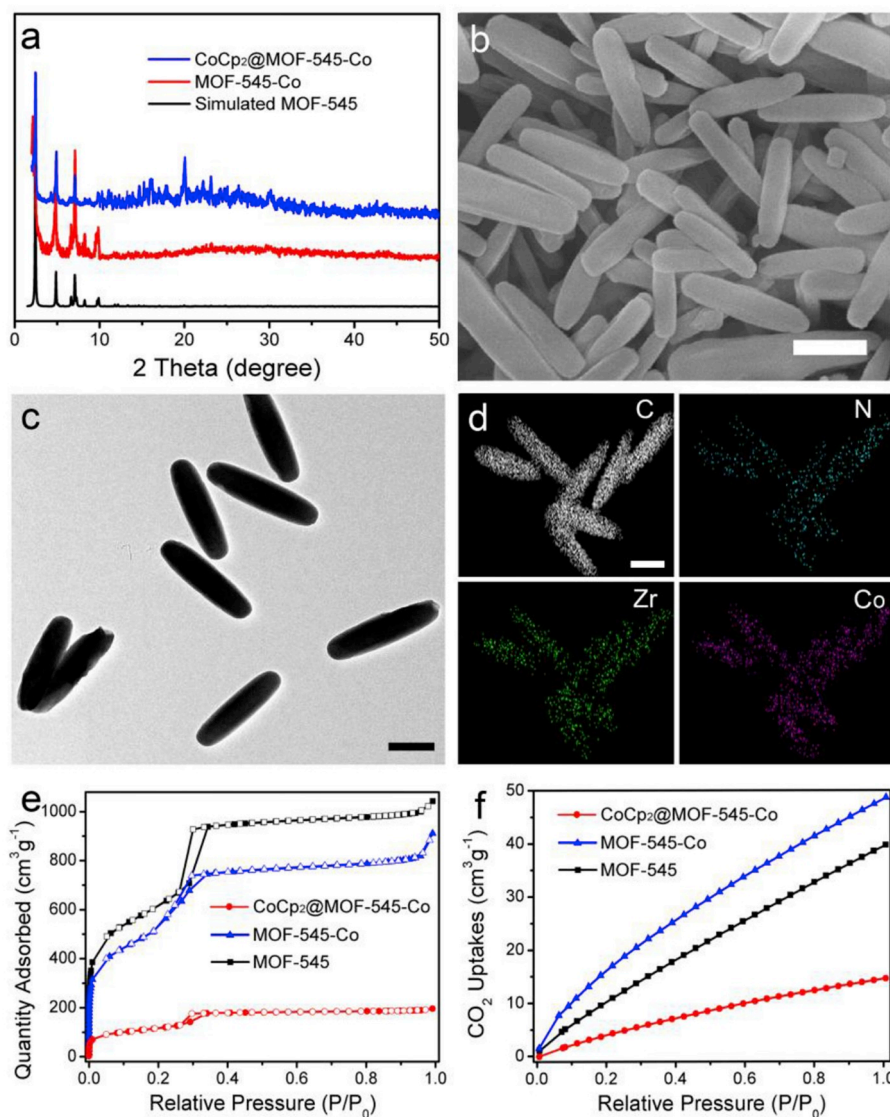
and carrier to enrich the electron density of MOF structure. The selected MOFs are quite important, to be cooperated with the properties of metallocene, the target ones would be better to have the functionality of carrying or accepting electrons. Metalloporphyrin based MOFs (e.g., MOF-545-Co) are promising alternatives, in which porphyrin ring is ideal charge transfer carrier and metal in the center of porphyrin ring might serve as efficient electron acceptor and active catalysis center [34]. The incorporation of metallocene with metalloporphyrin in MOF structure will presumably create electron transfer channel and might largely enhance the electron transfer ability or catalytic activity.

Herein a facile and versatile chemical vapor deposition protocol is proposed to introduce MCp$_2$ into MOF structure (Fig. 1) [35,36]. In this method, MCp$_2$ (M = Fe, Co, Ni) with diverse metal centers can be implanted into the pores of metalloporphyrin based MOF-545. MOF-545 imparting with high porosity, large pore size (3.6 nm) and excellent chemical and thermal stability can serve as ideal platform to interact with MCp$_2$. In the obtained MCp$_2$@MOF-545 composites, the π-electron system of cyclopentadienyl ring might overlap with π-electron system of porphyrin, which would endow MOF-545 with higher CO$_2$ adsorption capability, larger amount of active sites and more favorable electron transfer property to largely enhance the electrocatalytic CO$_2$RR activity (Fig. 1). As a proof-of-concept, MCp$_2$@MOF-545-Co exhibit excellent catalysis performances for CO$_2$RR. Specifically, CoCp$_2$@MOF-545-Co can selectively convert CO$_2$ to CO with 97% Faradaic efficiency for CO (FE$_{CO}$) and a detailed MCp$_2$ bonding mechanism is intensively discussed and revealed by density functional theory (DFT) calculation.

2. Experimental section

2.1. Syntheses of samples

Synthesis of MOF-545: MOF-545 was synthesized according to a referenced procedure [37]. ZrOCl$_2$·8H$_2$O (650 mg, 2.0 mmol) and

Fig. 2. Characterization of CoCp$_2$@MOF-545-Co. (a) PXRD patterns of CoCp$_2$@MOF-545-Co, MOF-545-Co and simulated MOF-545. (b) SEM image of CoCp$_2$@MOF-545-Co. (c) TEM image of CoCp$_2$@MOF-545-Co. (d) EDS elemental mapping of CoCp$_2$@MOF-545-Co. (e) N$_2$ sorption isotherms of CoCp$_2$@MOF-545-Co, MOF-545-Co and MOF-545. (f) CO$_2$ adsorption curves of CoCp$_2$@MOF-545-Co, MOF-545-Co and MOF-545 at 298 K. The scale bar presented in the figure is 200 nm.

tetrakis(4-carboxyphenyl)porphyrin (TCPP-H$_2$, 130 mg, 0.192 mmol) were dissolved in 160 mL of DMF and 5 mL of dichloroacetic acid in a 250 mL round-bottomed flask. The mixture was heated to 130 °C for 15 h with stirring, and allowed to cool to room temperature. The solid was collected by centrifugation, and washed with DMF until the liquid become colorless. And then the resulting powder was dispersed in a solution containing 50 mL of DMF and 5 mL of 1 M HCl and refluxed for 2 h. After centrifugation, the solid was washed with DMF and acetone for several times and then soaked in acetone overnight. The powder was washed with acetone and dried at 60 °C under vacuum. After drying, about 200 mg purple powder was collected (yield 85% based on TCPP-H$_2$).

Syntheses of various MOF-545-M: MOF-545 (50 mg) was dispersed in 10 mL DMF solution of CoCl$_2$·6H$_2$O (100 mg, 0.42 mmol). After sonicating for 10 min, the solution was heated at 100 °C for 20 h. After heating, purple powder was collected by centrifugation and washed with DMF for several times until the liquid become colorless. The DMF was replaced with acetone (5 × 30 mL) over a three-day period. Finally, the powder was dried in vacuum at 60 °C overnight. The preparation processes of MOF-545-Fe and MOF-545-Ni were similar to that of MOF-

545-Co except that CoCl$_2$·6H$_2$O was replaced by FeCl$_2$ (100 mg) and NiCl$_2$·6H$_2$O (100 mg), respectively [30].

Syntheses of various MCp$_2$@MOF-545-Co: CoCp$_2$@MOF-545-Co was synthesized by a modified chemical vapor deposition method [35,36]. CoCp$_2$ (20 mg) was placed in a round bottom flask and pre-activated MOF-545-Co (50 mg) in another round bottom flask with a suction valve, and then the two flask was connected with a glass elbow. The reaction system was placed in an oven at 40 °C and evacuated for 30 min. Then close the valve and keep the vacuum and temperature for 2 h. After cooling to room temperature, the reactor was filled with N$_2$ and then the sample was washed with N, N'-dimethylformamide (DMF) and acetone for three times. After drying under vacuum at 50 °C for 4 h, about 55 mg dark red powder was obtained. The preparation processes of FeCp$_2$@MOF-545-Co and NiCp$_2$@MOF-545-Co were similar to that of CoCp$_2$@MOF-545-Co except that FeCp$_2$ and NiCp$_2$ were used, respectively.

2.2. Material characterization

Powder X-ray diffraction (PXRD) experiments were recorded on a

Bruker D8 Advance (operating at 40 kV and 20 mA) with Ni-filtered Cu Ka radiation at 1.5406 (Å) with a speed of 5° min^{-1}. The thermo-gravimetric analysis (TGA) was carried out on a Shimadzu DTG-60H thermo-gravimetric analyzer in the air flow of 30 mL min^{-1} and the heating rate of 10 °C min^{-1}. SEM images and EDS were obtained from a FEI NOVA NANO 430 Field Emission Scanning Electron Microscope equipped with an Oxford Energy Dispersive X-ray spectroscopy. TEM images and STEM-HAADF images coupled to EDS elemental mapping were collected on a JEOL JEM-2100 electron microscope at 200 kV equipped with an Oxford Energy Dispersive X-ray spectroscopy. N_2 and CO_2 sorption measurements were carried out on a Micromeritics ASAP 2460 system at 77 K and 298 K, respectively, after the samples were first degassed at 120 °C for 8 h. X-ray Photoelectron Spectroscopy (XPS) was carried out on a Thermo ESCALAB 250XI multifunctional imaging electron spectrometer using the binding energy of C as the internal standard. The model for CoCp$_2$@MOF-545-Co, including CoCp$_2$ position, was generated using Materials Studio chemical structure-modeling software.

2.3. Electrochemical measurements

All electrochemical tests were performed in a standard three-electrode configuration in 0.5 M KHCO$_3$ solution using the electrochemical workstation (Bio-Logic). Carbon rod and Ag/AgCl were used as reference electrode and counter electrode, respectively, and modified carbon paper (1 cm × 1 cm) was used as work electrode. The electrochemical CO$_2$RR performance was carried out in an airtight electrochemical H-type cell, in which, two compartments were separated by a Nafion®117 proton exchange membrane to prevent the oxidation of CO$_2$ reduction products.

The catalyst-modified carbon paper electrode (denoted as CPE, 1 cm × 2 cm) was prepared as follows. 10 mg modified MOFs, 10 mg acetylene black (AB) were grounded together to form the uniform black powder. This black powder was dispersed into 1 mL 0.5% Nafion solution and sonication for 30 min to form uniform catalyst ink. Then, the ink was dropped directly onto a carbon paper (1 cm × 1 cm) with a catalyst loading density of ~1 mg cm^{-2} and dried at ambient temperature.

The polarization curves were performed by linear sweep voltammetry (LSV) mode at a scan rate of 5 mV s^{-1}. In this experiment, polarization curves were recorded successively in Ar-saturated and CO$_2$-saturated KHCO$_3$ solution.

The measurement of electrochemical impedance spectroscopy (EIS) is carried out under the overpotential of -0.7 V (relative to RHE). During the measurement process, 10 mV amplitude AC voltage is applied in the frequency range of 1000 kHz to 100 mHz. To estimate the electrochemical active surface area (ECSA), cyclic voltammograms (CV) were tested by measuring double-layer capacitance (Cdl) under the potential window of 0 V–0.1 V (vs. Ag/AgCl) with various scan rates from 100 to 200 mV s^{-1}. In this work, all the potentials are measured vs. Ag/AgCl electrode and the results are reported vs. reversible hydrogen electrode (RHE) based on the Nernst equation: E (vs. RHE) = E (vs. Ag/AgCl) + 0.1989 V + 0.059 × pH (without iR compensation).

3. Results and discussion

MCp$_2$@MOF-545-Co samples are prepared by chemical vapor deposition (CVD) method. In the structure of MOF-545-Co, Zr$_6$O$_8$ clusters are linked by Co-TCPP ligands to generate two kind of pores with diameters about 16 Å and 36 Å [34,37], which is large enough to encapsulate MCp$_2$ molecules (about 3.5 Å × 4.5 Å) [35]. Taking the preparation of CoCp$_2$@MOF-545-Co for example, the CoCp$_2$ can be evaporated into the pre-evacuated pores of MOF-545-Co under vacuum condition at 40 °C. After the CVD process, the sample is washed with N, N′-dimethylformamide (DMF) and acetone for several times and dried under vacuum for further characterization.
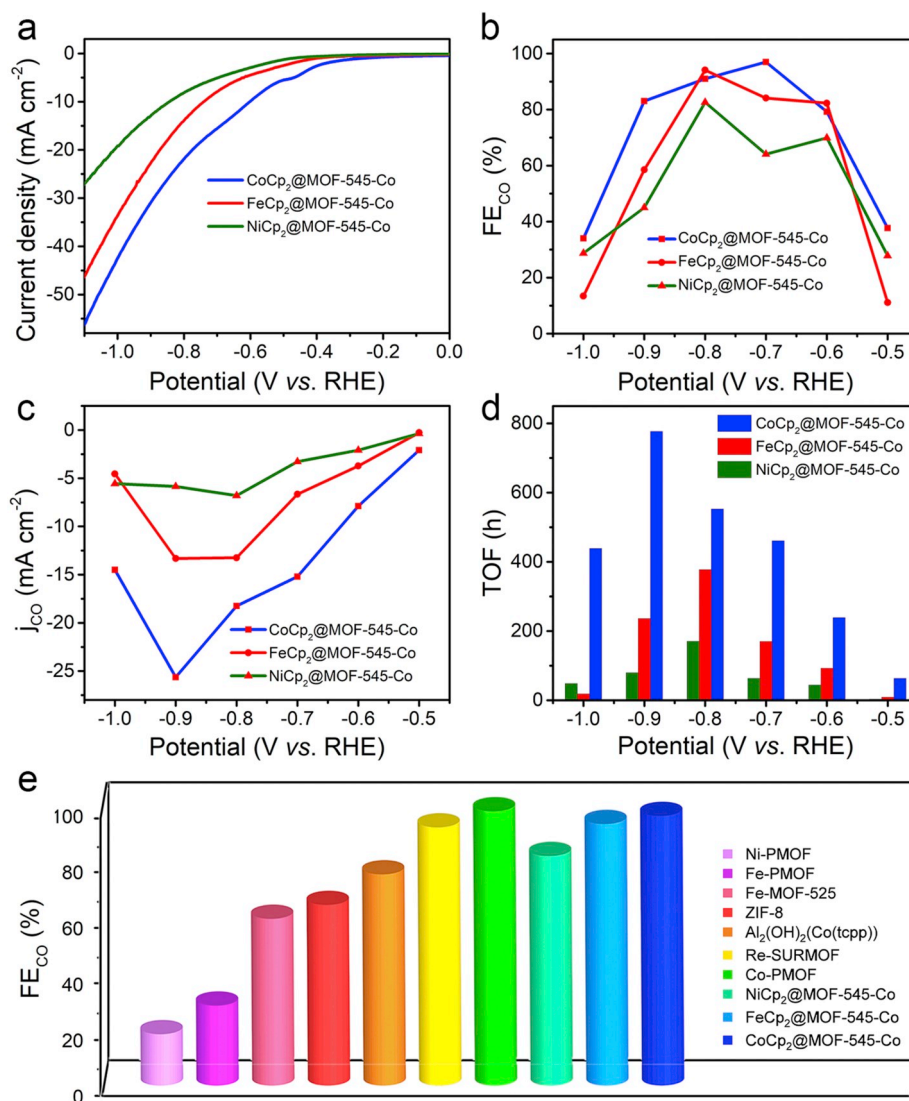
Powder X-ray diffraction (PXRD) tests confirm that the structure of MOF-545-Co remains intact after implantation of CoCp$_2$ (Fig. 2a). Scanning electron microscope (SEM) tests show that the as-prepared CoCp$_2$@MOF-545-Co displays rod-like morphology, and the average diameter calculated through a Nano-measurer software is about 92 nm (Fig. 2b). The smooth surface of the rods can get rid of the possibility of the recrystallization of CoCp$_2$ on the surface of MOF-545-Co. Similar results are also detected in transmission electron microscope (TEM) tests (Fig. 2c). Moreover, C, N, Zr and Co are uniformly dispersed in rod-like crystals of MOF-545-Co as presented in the energy dispersive X-ray spectroscopy (EDS) elemental mapping characterization (Fig. 2d). The composition of CoCp$_2$@MOF-545-Co is further detected and the Zr/Co ratio in CoCp$_2$@MOF-545-Co is about 3:2, which is higher than that of MOF-545-Co (3:1) (Fig. S1). It can be calculated that about 6 CoCp$_2$ molecules are loaded in each unit cell of MOF-545-Co and the mole ratio of CoCp$_2$ and Co-TCPP is about 1:1. The Co contents in CoCp$_2$@MOF-545-Co and MOF-545-Co are calculated based on XPS data. The Co contents in MOF-545-Co and CoCp$_2$@MOF-545-Co are detected to be 1.22% and 2.52%, respectively (Fig. S11). The value of CoCp$_2$@MOF-545-Co is about twice than that of MOF-545-Co. Besides, the mole ratio of CoCp$_2$ and Co-TCPP in CoCp$_2$@MOF-545-Co is about 1 : 1, which is consistent with EDS results. To investigate the versatility of the strategy, NiCp$_2$@MOF-545-Co and FeCp$_2$@MOF-545-Co are also successfully prepared following the same procedures and proved by PXRD, SEM, TEM and EDS mapping tests (Figs. S2–6). The average diameters of MOF-545-Co, FeCp$_2$@MOF-545-Co and NiCp$_2$@MOF-545-Co are calculated to be about 90, 91 and 92 nm, respectively.

To investigate elemental states of MCp$_2$ compounds in the pore of MOF-545-Co, X-ray photoelectron spectra (XPS) of MCp$_2$@MOF-545-Co is performed to determine its surface electronic states and elemental compositions (Fig. S7). As depicted in Fig. S8, XPS spectra of CoCp$_2$@-MOF-545-Co suggest the existence of C, N, O, Zr and Co. The high-resolution Co 2p spectra are fitted into two peaks at 781.3 and 796 eV, which are attributed to Co 2p$_{3/2}$ for CoCp$_2$ and Co 2p$_{1/2}$ for Co^{2+}, respectively [38,39]. For FeCp$_2$@MOF-545-Co, the peaks at 707.8 and 707.4 eV are fitted into Fe 2p$_{3/2}$ for FeCp$_2$ and Fe 2p$_{1/2}$ for Fe^{2+}, respectively (Fig. S9) [40,41]. Similarly, the peaks of NiCp$_2$@-MOF-545-Co located at 856.10 and 873.70 eV are attributed to the Ni 2p$_{3/2}$ for NiCp$_2$ and Ni 2p$_{1/2}$ for Ni^{2+}, respectively (Fig. S10) [42–44].

N_2 sorption tests are conducted to evaluate the porosity of obtained materials. Brunauer-Emmett-Teller (BET) surface areas of MOF-545, MOF-545-Co and CoCp$_2$@MOF-545-Co are calculated to be 2204, 2126 and 663 m^2 g^{-1}, respectively (Fig. 2e). The BET value of CoCp$_2$@MOF-545-Co is decreased coupling with the weaker peak intensity in the pore size distribution after the loading of CoCp$_2$ (Fig. S12, Table S1). To further support the porosity of the obtained samples, CO$_2$ adsorption measurements are performed. The CO$_2$ adsorption values are 39, 48 and 16 cm^3 g^{-1} for MOF-545, MOF-545-Co, and CoCp$_2$@MOF-545-Co at 298 K, respectively (Fig. 2f). CoCp$_2$@MOF-545-Co can absorb 6 CO$_2$ molecules per unit cell at 1 atm and 298 K, which would be beneficial for efficient electrocatalytic CO$_2$RR. Besides, CoCp$_2$@MOF-545-Co presents CO$_2$ adsorption capacity of 23.9 cm^3 g^{-1} at 273 K and 19.3 cm^3 g^{-1} at 283 K, respectively. The adsorption enthalpy of CoCp$_2$@MOF-545-Co is calculated to be 30.1 kJ mol^{-1} (Fig. S13).

Stability is a crucial factor for materials to be evaluated for further applications. To investigate the chemical stability of CoCp$_2$@MOF-545-Co, the sample is soaked in KHCO$_3$ aqueous solution (0.5 M) for more than 24 h. PXRD pattern shows that the structure of CoCp$_2$@MOF-545-Co remains intact before and after soaking in KHCO$_3$ aqueous solution (Fig. S14). As proved by the EDS analysis, the ratio of Zr/Co after soaking in KHCO$_3$ aqueous solution for 24 h is similar as that of sample before test, revealing the high chemical stability of CoCp$_2$@MOF-545-Co (Table S2).

The thermal stability of CoCp$_2$@MOF-545-Co is further studied by thermogravimetric analysis (TGA) in air with a heating rate of 10 °C min^{-1}. CoCp$_2$@MOF-545-Co can be stable at temperature up to 350 °C
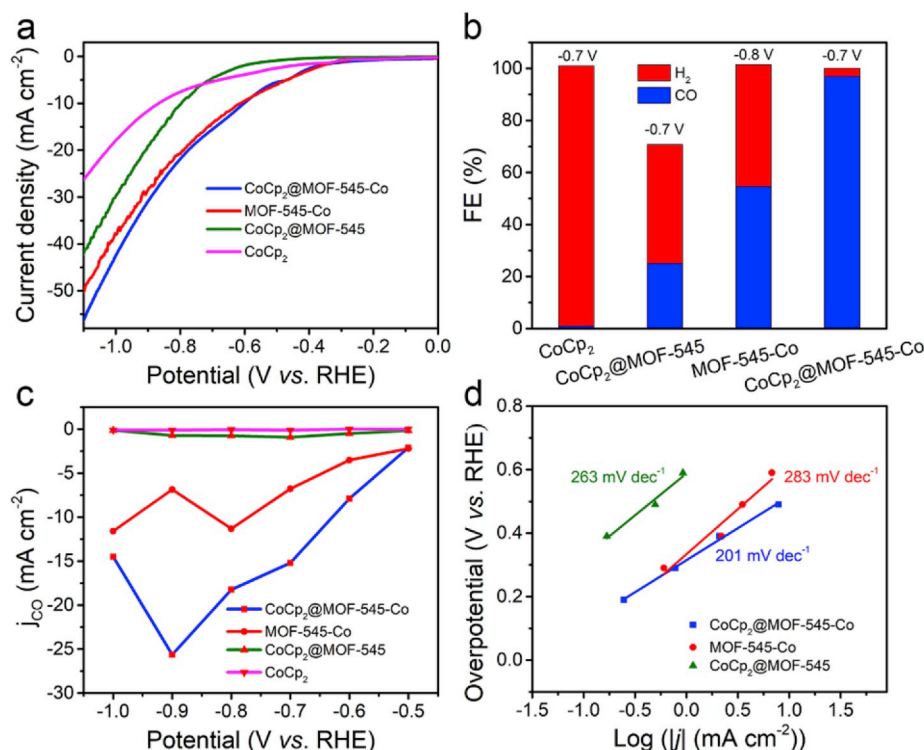
Fig. 3. Electrocatalytic CO$_2$RR performances of MCp$_2$@MOF-545-Co.(a) Linear sweep voltammetric curves. (b) Faradaic efficiencies for CO at different potentials. (c) Partial CO current density. (d) TOFs. (e) Electrocatalytic CO$_2$RR performances of MCp$_2$@MOF-545-Co and other electrocatalysts.

(Fig. S15). The high chemical and thermal stability of CoCp$_2$@MOF-545-Co set fundamental basis for its future investigations in electrocatalytic CO$_2$RR.The electrocatalytic CO$_2$RR is evaluated in a three-electrode system in CO$_2$-saturated 0.5 M KHCO$_3$ (pH = 7.2) solution. The catalytic performances of MOF-545-Co, MOF-545-Fe and MOF-545-Ni are evaluated and corresponding FE$_{CO}$ or FE$_{H2}$ over the entire potential range are calculated. MOF-545-Co has a smaller onset potential and a higher FE$_{CO}$ value (−0.32 V, 54.6%) than MOF-545-Fe (−0.35 V, 9.4%) and MOF-545-Ni (−0.61 V, 14.1%). The higher CO$_2$RR performance of MOF-545-Co than MOF-545-Fe/Ni is similar to previous reports (Fig. S16) [29]. Therefore, we select MOF-545-Co as the desired substrate to load MCp$_2$.

After loading of CoCp$_2$, CoCp$_2$@MOF-545-Co presents a low onset potential of −0.27 V and a large total current density of 56.2 mA cm^{-2} at −1.1 V in the linear sweep voltammetry (LSV) curves (Fig. 3a). In Ar-saturated KHCO$_3$ solution, CoCp$_2$@MOF-545-Co shows a much smaller current density than that in CO$_2$-saturated KHCO$_3$ solution, indicating the high electrochemical performance of CoCp$_2$@MOF-545-Co indeed come from CO$_2$RR (Fig. S17). To further detect the CO$_2$RR selectivity of these samples, the FE tests are carried out. CO and H$_2$ are the main gas products monitored by the GC test and there is no liquid product detected in the ^{1}H NMR spectroscopy (Fig. S18). CoCp$_2$@MOF-545-Co

maintains excellent FE$_{CO}$ (>80%) in a wide potential range (from −0.6 to −0.9 V) and can reach up to a maximum value of 97% at −0.7 V (Fig. 3b). Moreover, CoCp$_2$@MOF-545-Co with diverse CoCp$_2$ loadings are synthesized and present FE$_{CO}$ values of 54% (CoCp$_2$@MOF-545-Co-0.5, the mole ratio of CoCp$_2$ and Co-TCPP is 0.5) and 59% (CoCp$_2$@-MOF-545-Co-2, the mole ratio of CoCp$_2$ and Co-TCPP is 2) at −0.7 V, respectively (Fig. S19). To modify the conductivity of the materials, we have applied diverse loadings of acetylene black to test the best performance. With the ratio of catalyst to acetylene black tuned from 2 : 1 to 1 : 2, the FE$_{CO}$ values and potential range of the materials change accordingly (Fig. S20). The best ratio of catalyst to acetylene black is 1 : 1.

As comparison, FeCp$_2$@MOF-545-Co and NiCp$_2$@MOF-545-Co have a maximum FE$_{CO}$ value of 94.1 and 82.6% at −0.8 V, respectively (Fig. 3b). The catalytic performance of CoCp$_2$@MOF-545-Co is higher than comparisons and outperforms most of MOF based catalysts (Fig. 3e; Table S3). The partial CO current density is performed to reveal the activity of the samples. CoCp$_2$@MOF-545-Co exhibits a high value of −25.63 mA cm^{-2} at −0.9 V, almost twice higher than FeCp$_2$@MOF-545-Co (−13.32 mA cm^{-2}, -0.9 V) and NiCp$_2$@MOF-545-Co (−5.85 mA cm^{-2}, -0.9 V) (Fig. 3c). Besides, the turnover frequency (TOF) of CoCp$_2$@MOF-545-Co is calculated to be 777 h^{-1} at −0.9 V,

Fig. 4. Fig. 4 Electrocatalytic CO_2RR performances of contrast samples for CoCp$_2$@MOF-545-Co.(a) Linear sweep voltammetric curves. (b) Faradaic efficiencies for CO and H$_2$. (c) Partial CO current density. (d) Tafel plots. These tests are performed in 0.5 M KHCO$_3$ electrolyte with a scan rate of 5 mV s^{-1}.

which is superior to FeCp$_2$@MOF-545-Co (377.9 h^{-1}, -0.8 V) and NiCp$_2$@MOF-545-Co (170.4 h^{-1}, -0.8 V) (Fig. 3d).

To study the accurate catalytic site for CoCp$_2$@MOF-545-Co in electrocatalytic CO_2RR, a series of contrast samples (i.e. MOF-545-Co, CoCp$_2$ and CoCp$_2$@MOF-545) are prepared to test their electro-catalysis performances for CO_2RR. CoCp$_2$MOF-545-Co exhibits a smaller onset potential and a larger total current density than CoCp$_2$@MOF-545, MOF-545-Co and CoCp$_2$ (Fig. 4a, c). Furthermore, the corresponding maximum FE$_{CO}$ values for CoCp$_2$@MOF-545-Co, MOF-545-Co, CoCp$_2$@MOF-545 and CoCp$_2$ are 97%, 54.6%, 19.8% and 1%, respectively (Fig. 4b; S21). As revealed, MOF-545-Co shows poorer CO_2 reduction performance than CoCp$_2$@MOF-545-Co, which might be ascribed to the lower electron transfer efficiency. In contrast, CoCp$_2$@MOF-545 has negligible CO_2 reduction activity and CoCp$_2$ shows almost no activity for CO_2RR but predominantly hydrogen evolution reaction (HER), implying the excellent CO_2 reduction performance of CoCp$_2$@MOF-545-Co originates from the synergy effect of MOF-545-Co and CoCp$_2$. To further support the catalytic mechanism, FeCp$_2$ and NiCp$_2$ are tested as contrast samples for FeCp$_2$@MOF-545-Co and NiCp$_2$@MOF-545-Co, respectively. As expected, FeCp$_2$ and NiCp$_2$ display negligible electrocatalytic CO_2RR activity (Fig. S22).
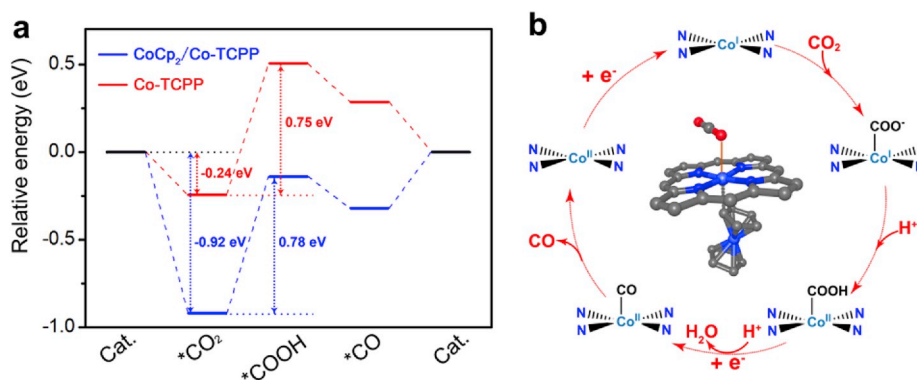
The reaction kinetics for the CO formation is elucidated by the Tafel slopes (Fig. 4d). Remarkably, the Tafel slope for CoCp$_2$@MOF-545-Co is 201 mV dec^{-1}, which is lower than that of MOF-545-Co (283 mV dec^{-1}) and CoCp$_2$@MOF-545 (263 mV dec^{-1}), demonstrating more favorable kinetics of CoCp$_2$@MOF-545-Co for the generation of CO. The Tafel slope of CoCp$_2$@MOF-545-Co is reasonable and among the values reported for porphyrin based coordination polymers (e.g., MOFs or COFs) for CO_2RR [29,45].

To further probe the potential influence factors for the excellent performance of CoCp$_2$@MOF-545-Co, the electrochemical double layer capacitance (C$_{dl}$) is also calculated to estimate the electrochemical active surface area (ECSA) (Fig. S23). Specifically, CoCp$_2$@MOF-545-Co exhibits larger C$_{dl}$ value (7.26 mF cm^{-2}) than MOF-545-Co (6.28 mF cm^{-2}), CoCp$_2$@MOF-545 (6.83 mF cm^{-2}) and CoCp$_2$

(2.17 mF cm^{-2}), indicating its larger effective electrochemical area for electrocatalysis among these samples, which might provide more active sites to contact with the reactant to accelerate the electrocatalytic CO_2RR process. Moreover, electrochemical impedance spectroscopy (EIS) is performed to study the electrode reaction kinetics in the electrocatalysis process. As revealed by the Nyquist plots, the charge transfer resistance (Rct) of CoCp$_2$@MOF-545-Co (7.48 Ω) is significantly lower than that of MOF-545-Co (23.23 Ω), CoCp$_2$@MOF-545 (22.82 Ω) and CoCp$_2$ (31.59 Ω), implying the faster charge transfer rate for CoCp$_2$@-MOF-545-Co (Fig. S24). Besides, the current density of CoCp$_2$@MOF-545-Co (-25.63 mA cm^{-2} at -0.9 V) is largely increased compared with MOF-545-Co (-6.94 mA cm^{-2} at -0.9 V), which indicates that the introduction of CoCp$_2$ indeed improves the conductivity of the MOF material (Fig. 4c). Further proved by the conductivity test, the implantation of CoCp$_2$ can enhance the conductivity of MOF-545-Co (Fig. S25). To evaluate the electrocatalysis stability, PXRD and SEM tests of CoCp$_2$@MOF-545-Co after electrocatalytic reaction are performed. The remained intact topology and almost unchanged morphology suggest that CoCp$_2$@MOF-545-Co exhibits high stability during electrocatalytic reaction (Figs. S26 and S27).

To further investigate the electrocatalytic CO_2RR mechanism of CoCp$_2$@MOF-545-Co, DFT calculations are performed. Generally, the equilibrium of 6 CoCp$_2$ molecules in one unit cell of MOF-545-Co (42.68 × 42.68 × 16.66 Å^3) is obtained by 10^8 steps of Monte Carlo simulations in NVT ensemble (the isothermal-isasteric ensemble) using Music code (the detailed information of the simulated structure see Fig. S26 [46,47]. The van der Waals interaction is described by Lennard-Jones (LJ) potential using UFF force field [48], and the electrostatic interaction is calculated based on ESP charge [49] for CoCp$_2$ and QEq charge [50] for the framework. The Lennard-Jones (LJ) parameters are listed in Table S4 and the charge of CoCp$_2$ is presented in Fig. S26b. CoCp$_2$ tends to be adsorbed in the triangle channel, as well as beside the zircon-oxygen clusters. Furthermore, the mechanism of CoCp$_2$ adsorbed on Co-TCPP is studied to model the possible interaction in MOF-545-Co. Interestingly, strong chemical bond is found between C

Fig. 5. Fig. 5 The DFT calculation and proposed catalysis mechanism of $CoCp_2$@MOF-545-Co. (a) The free energy diagrams of CO_2 reduction to CO for Co-TCPP (red line) and $CoCp_2$ decorated Co-TCPP (blue line). (b) Proposed reaction mechanism of electrocatalytic CO_2RR on $CoCp_2$@MOF-545-Co.

of $CoCp_2$ and Co of Co-TCPP during electrocatalytic CO_2RR in $CoCp_2$@MOF-545-Co (Fig. 5 and S28a).

To reveal the specific effects of $CoCp_2$ and Co-TCPP for electrocatalytic CO_2RR, we adopt finite cluster calculations for the MOF framework to reduce the computation time effectively, as we assume the long range interaction for each local center is trivial. In the case of CO_2RR on a single porphyrin structure as presented in Fig. 5, the interaction between CO_2 and Co center is rather weak, and the binding energy is calculated to be -0.24 eV, which is in the range of weak van der Walls interaction (Fig. 5a). The first hydrogenation process (from *CO_2 to *COOH) after the adsorption of CO_2 serves as the potential-determining step and the free energy of 0.75 eV is obtained. As the second electron and proton inject into the unit, *COOH finally turns into CO molecules and desorbs into the environment. With the adsorption of $CoCp_2$ on Co-TCPP, the adsorption energy of CO_2 can be largely reduced to -0.92 eV. Although the potential-determining step from *CO_2 to *COOH remains as 0.78 eV, the strong interaction between the reactant and substrate can lead to much improved efficiency and selectivity for the generation of CO. Further supported by the better electrocatalytic performance of $CoCp_2$@MOF-545-Co (FE_{CO}, 97%) compared with MOF-545-Co (FE_{CO}, 54.6%), the strong interaction between the reactant and substrate (almost four times increase in CO_2 adsorption energy) indeed has positive effect on the performance. Above all, the introduction of $CoCp_2$ can: 1) serve as electron donor and carrier to enrich the electron density of MOF structure; 2) form C–Co bond with Co-TCPP during CO_2RR electrocatalysis to largely reduce the adsorption energy of CO_2; 3) create continuous electron transfer channel to improve the electron migration of MOFs and increase the CO_2RR efficiency.

Except for $CoCp_2$@MOF-545-Co, the free energy diagrams of $FeCp_2$@MOF-545-Co and $NiCp_2$@MOF-545-Co are also evaluated by DFT calculations (Fig. S29). The adsorption energy values of $FeCp_2$@MOF-545-Co (-0.72 eV) and $NiCp_2$@MOF-545-Co (-0.71 eV) for carbon dioxide are lower than $CoCp_2$@MOF-545-Co (-0.92 eV). The more negative adsorption free energy makes CO_2 more likely to be adsorbed on $CoCp_2$@MOF-545-Co to exhibit higher electron transfer efficiency and better performance in electrocatalytic CO_2RR. Further supported by the electrocatalytic CO_2RR performances, $CoCp_2$@MOF-545-Co (FE_{CO} 97%, -0.7 V; -25.63 mA cm^{-2}, -0.9 V) presents higher FE_{CO} and current density than $FeCp_2$@MOF-545-Co (FE_{CO} 94.1%, -0.8 V; -13.32 mA cm^{-2}, -0.9 V) and $NiCp_2$@MOF-545-Co (FE_{CO} 82.6%, -0.8 V; -5.85 mA cm^{-2}, -0.9 V) (Fig. 3c).

4. Conclusions

In summary, a facile and versatile chemical vapor deposition protocol is reported to introduce metallocene into MOFs. In this method, metallocene with diverse metal centers have been implanted into the pores of metalloporphyrin based MOF-545-Co. Thus-obtained MCp_2@MOF-545-Co (M = Fe, Co, Ni) composites can efficiently combine the advantages of MCp_2 and MOF-545-Co to present excellent catalysis performance in electrocatalytic CO_2RR. Specifically, $CoCp_2$@MOF-545-Co can selectively convert CO_2 to CO with a high FE_{CO} of 97% and the result is superior to most of reported MOFs. The high performances might be attributed to the strong binding-interaction between metallocene and metalloporphyrin (e.g., C–Co between $CoCp_2$ and Co-TCPP in $CoCp_2$@MOF-545-Co) as revealed by DFT calculations. The introduction of metallocene can serve as electron donor and carrier to create continuous electron transfer channel in MOFs and the strong binding-interaction with metalloporphyrin during CO_2RR process can largely reduce the adsorption energy of CO_2 to enhance the activity. This strategy paves a new way to improve the CO_2RR efficiency of MOFs and might shed light on the development of highly selective CO_2RR electrocatalysts.

Appendix A. Supplementary data

Supplementary data to this article can be found online at https://doi.org/10.1016/j.nanoen.2019.104233.

References

[1] J.D. Shakun, P.U. Clark, F H, Shaun A. Marcott, A.C. Mix, Z. Liu, B. Otto-Bliesner, A. Schmittner, E. Bard, Nature 484 (2012) 49–54.
[2] K. Sumida, D.L. Rogow, J.A. Mason, T.M. McDonald, E.D. Bloch, Z.R. Herm, T.-H. Bae, J.R. Long, Chem. Rev. 112 (2012) 724–781.
[3] J. Qiao, Y. Liu, F. Hong, J. Zhang, Chem. Soc. Rev. 43 (2014) 631–675.
[4] P.-Q. Liao, J.-Q. Shen, J.-P. Zhang, Coord. Chem. Rev. 373 (2018) 22–48.
[5] Y. Pan, R. Lin, Y. Chen, S. Liu, W. Zhu, X. Cao, W. Chen, K. Wu, W.-C. Cheong, Y. Wang, L. Zheng, J. Luo, Y. Lin, Y. Liu, C. Liu, J. Li, Q. Lu, X. Chen, D. Wang, Q. Peng, C. Chen, Y. Li, J. Am. Chem. Soc. 140 (2018) 4218–4221.
[6] J. Jiao, R. Lin, S. Liu, W.-C. Cheong, C. Zhang, Z. Chen, Y. Pan, J. Tang, K. Wu, S.-F. Hung, H.M. Chen, L. Zheng, Q. Lu, X. Yang, B. Xu, H. Xiao, J. Li, D. Wang, Q. Peng, C. Chen, Y. Li, Nat. Chem. 11 (2019) 222–228.
[7] H. Rao, L.C. Schmidt, J. Bonin, M. Robert, Nature 548 (2017) 74–77.
[8] P.D. Luna, R. Quintero-Bermudez, C.-T. Dinh, M.B. Ross, O.S. Bushuyev, P. Todorović, T. Regier, S.O. Kelley, P. Yang, E.H. Sargent, Nat. Catal. 1 (2018) 103–110.
[9] T. Haas, R. Krause, R. Weber, M. Demler, G. Schmid, Nat. Catal. 1 (2018) 32–39.
[10] D.D. Zhu, J.L. Liu, S.Z. Qiao, Adv. Mater. 28 (2016) 3423–3452.

[11] S. Zhao, Y. Wang, J. Dong, C.-T. He, H. Yin, P. An, K. Zhao, X. Zhang, C. Gao, L. Zhang, J. Lv, J. Wang, J. Zhang, A.M. Khattak, N.A. Khan, Z. Wei, J. Zhang, S. Liu, H. Zhao, Z. Tang, Nature Energy 1 (2016) 16184–16193.

[12] Q. Li, J. Fu, W. Zhu, Z. Chen, B. Shen, L. Wu, Z. Xi, T. Wang, G. Lu, J.-J. Zhu, S. Sun, J. Am. Chem. Soc. 139 (2017) 4290–4293.

[13] W. Zhang, Y. Hu, L. Ma, G. Zhu, Y. Wang, X. Xue, R. Chen, S. Yang, Z. Jin, Adv. Sci. 5 (2018) 1700275.

[14] S. Gao, Y. Lin, X. Jiao, Y. Sun, Q. Luo, W. Zhang, D. Li, J. Yang, Y. Xie, Nature 529 (2016) 68–71.

[15] M. Asadi, C. Liu, A. Addepalli, P. Abbasi, P. Yasaei, P. Phillips, A. Behranginia, J. Cerrato, R. Haasch, P. Zapo, B. Kumar, R. Klie, J. Abiade, L. Curtiss, A. Salehi-Khojin, Science 353 (2016) 467–470.

[16] X. Duan, J. Xu, Z. Wei, J. Ma, S. Guo, S. Wang, H. Liu, S. Dou, Adv. Mater. 29 (2017) 1701784.

[17] Z. Sun, T. Ma, H. Tao, Q. Fan, B. Han, Chemicals 3 (2017) 560–587.

[18] S. Zhao, D.-W. Wang, R. Amal, L. Dai, Adv. Mater. 31 (2019) 1801526.

[19] L. Ye, J. Liu, Y. Gao, C. Gong, M. Addicoat, T. Heine, C. Wöll, L. Sun, J. Mater. Chem. A 4 (2016) 15320–15326.

[20] Y. Wang, P. Hou, Z. Wang, P. Kang, ChemPhysChem 18 (2017) 3142–3147.

[21] L. Marleny R. Albelo, A.R. Ruiz-Salvador, A. Sampieri, D.W. Lewis, A. Gómez, B. Nohra, P. Mialane, J. Marrot, F. Sécheresse, C. Mellot-Draznieks, R.N. Biboum, B. Keita, L. Nadjo, A. Dolbecq, J. Am. Chem. Soc. 131 (2009) 16078–16087.

[22] R.S. Kumar, S.S. Kumar, M.A. Kulandainathan, Electrochem. Commun. 25 (2012) 70–73.

[23] Z. Liang, C. Qu, W. Guo, R. Zou, Q. Xu, Adv. Mater. 30 (2018) 1702891.

[24] X. Wang, Z. Chen, X. Zhao, T. Yao, W. Chen, R. You, C. Zhao, G. Wu, J. Wang, W. Huang, J. Yang, X. Hong, S. Wei, Y. Wu, Y. Li, Angew. Chem. Int. Ed. 57 (2018) 1944–1948.

[25] N. Kornienko, Y. Zhao, C.S. Kley, C. Zhu, D. Kim, S. Lin, C.J. Chang, O.M. Yaghi, P. Yang, J. Am. Chem. Soc. 137 (2015) 14129–14135.

[26] I. Hod, M.D. Sampson, P. Deria, C.P. Kubiak, O.K. Farha, J.T. Hupp, ACS Catal. 5 (2015) 6302–6309.

[27] D.-Y. Du, J.-S. Qin, S.-L. Li, Z.-M. Su, Y.-Q. Lan, Chem. Soc. Rev. 43 (2014) 4615–4632.

[28] D.-H. Nam, O.S. Bushuyev, J. Li, P.D. Luna, A. Seifitokaldani, C.-T. Dinh, F.P.G. de Arquer, Y. Wang, Z. Liang, A.H. Proppe, C.S. Tan, P. Todorović, O. Shekhah, C. M. Gabardo, J. Am. Chem. Soc. 140 (2018) 11378–11386.

[29] Y.-R. Wang, Q. Huang, C.-T. He, Y. Chen, J. Liu, F.-C. Shen, Y.-Q. Lan, Nat. Commun. 9 (2018) 4466.

[30] X. Kang, Q. Zhu, X. Sun, J. Hu, J. Zhang, Z. Liu, B. Han, Chem. Sci. 7 (2016) 266–273.

[31] C.W. Kung, C.-W. Kung, C.O. Audu, A.W. Peters, H. Noh, O.K. Farha, J.T. Hupp, ACS Energy Lett 2 (2017) 2394–2401.

[32] S. Dou, J. Song, S. Xi, Y. Du, J. Wang, Z.-F. Huang, Z. Xu, X. Wang, Angew. Chem. Int. Ed. 58 (2019), https://doi.org/10.1002/anie.201814711.

[33] H. Atzkern, B. Huber, F.H. Kohler, G. Müller, R. Müller, Organometallics 10 (1991) 238–244.

[34] W. Morris, V. Boris, D. Selcuk, G. Felipe, L. Psaras, G. Mc, F. Hiroyasu, C. Duilio, J. F. Stoddart, O.M. Yaghi, Inorg. Chem. 51 (2012) 6443–6445.

[35] S. Hermes, F. Schröter, S. Amirjalayer, R. Schmid, R.A. Fischer, J. Mater. Chem. 16 (2006) 2464–2472.

[36] S. Hermes, M.-K. Schröter, R. Schmid, L. Khodeir, M. Muhler, A. Tissler, R. W. Fischer, R.A. Fischer, Angew. Chem. Int. Ed. 44 (2005) 6237–6241.

[37] P. Grégoire, G.-M. Maria, R.-M. Catherine, L.-K. Benedikt, M. Pierre, F. Marc, M.-D. Caroline, J. Am. Chem. Soc. 140 (2018) 3613–3618.

[38] Ji-G. Li, R. Büchel, M. Isobe, T. Mori, T. Ishigaki, J. Phys. Chem. C 113 (2009) 8009–8015.

[39] L. Hernan, J. Morales, L. Sanchez, J.L. Tirado, Chem. Mater. 7 (1995) 1576–1582.

[40] M. Mullet, V. Khare, C. Ruby, Surf. Interface Anal. 40 (2008) 323–328.

[41] E.A. Dalchiele, A. Aurora, G. Bernardini, F. Cattaruzza, A. Flamini, P. Pallavicini, R. Zanoni, F. Decker, J. Electroanal. Chem. 579 (2005) 133–142.

[42] Y. An, B. Huang, Z. Wang, X. Long, Y. Qiu, J. Hu, D. Zhou, H. Lin, S. Yang, Dalton Trans. 10 (2017) 1820–1827.

[43] F.-C. Shen, S.-N. Sun, Z.-F. Xin, S.-L. Li, L.-Z. Dong, Q. Huang, Y.-R. Wang, Y.-Q. Lan, Appl. Catal. B Environ. 243 (2019) 470–480.

[44] M.V. Kharlamova, C. Kramberger, M. Sauer, K. Yanagi, T. Saito, T. Pichler, Appl. Phys. A 124 (2018) 247.

[45] S. Lin, C.S. Diercks, Y.-B. Zhang, N. Kornienko1, E.M. Nichols, Y. Zhao, A.R. Paris, D. Kim, P. Yang, O.M. Yaghi, C.J. Chang, Science 349 (2015) 1208–1213.

[46] S. Chempath, T. Düren, L. Sarkisov, R.Q. Snurr, Mol. Simul. 39 (2013) 1223–1232.

[47] A. Gupta, S. Chempath, M.J. Sanborn, L.A. Clark, R.Q. Snurr, Mol. Simul. 29 (2003) 29–46.

[48] A.K. Rappé, C.J. Casewit, K.S. Colwell, W.A. Goddard, W.M. Skiff, J. Am. Chem. Soc. 114 (1992) 10024–10035.

[49] C.I. Bayly, P. Cieplak, W.D. Cornell, P.A. Kollman, J. Phys. Chem. 97 (1993) 10269–10280.

[50] A.K. Rappé, W.A. Goddard Iii, J. Phys. Chem. 95 (1991) 3358–3363.

Zhi-Feng Xin was born in 1978 in Hebei, P. R. China. He received his Master degree in 2006 under the supervision of Prof. Jun Peng from Northeast Normal University. In 2010, he received his Ph.D. degree under the supervision of Prof. Junfeng Bai from Nanjing University. From 2010 to now, he worked at Anhui University of Technology. In 2017 he joined Prof. Ya-Qian Lan's group for the postdoctoral study. His research interest is related to the application of MOF nanomaterials in electrocatalysis of CO_2RR.
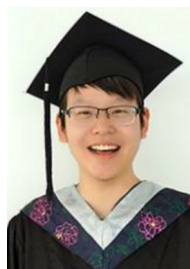

Yi-Rong Wang received her undergraduate degree (2016) and B.S. degree (2019) in Harbin Normal University and Nanjing Normal University, respectively, and now she is a Ph.D. candidate in Nanjing Normal University. Her current research focuses on the synthesis of MOFs-based hybrid electrocatalysts for electrocatalytic reduction of carbon dioxide.

Yifa Chen was born in 1989 in Fujian, P. R China. He received his B.S. degree from Beijing Institute of Technology. He subsequently obtained his Ph.D. degree from Beijing Institute of Technology under the supervision of Prof. Bo Wang. In 2018, he joined Prof. Ya-Qian Lan's group as an associate professor at Nanjing Normal University. His research interest focuses on the fabrication of Metal-Organic Framework (MOF) based devices like membranes, foams and fibers that can be applicable in energy storage and conversion, proton conductivity or photo/electric heterogeneous catalysis.
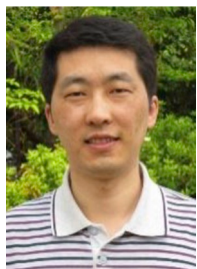

Wenliang Li obtained doctoral degree in 2012 under the supervision of Prof. Jingping Zhang from Northeast Normal University. In 2010 to 2011, he studied in University of Münster in Germany as a visiting scholar following Prof. Stefan GRIMME. From 2018 to 2019, he worked as a research fellow in Fukui Institute for Fundamental Chemistry (FIFC) in Shigeyoshi SAKAKI group, Kyoto University in Japan. His current research focuses on theoretical modeling of gas adsorption in porous materials, Li ion battery, and reactions on 2D surface.

Long-Zhang Dong was born in 1994 in Hebei, P. R. China. He received his BS degree in chemistry in 2017 from Nanjing Normal University. He is studying for a PhD degree in Nanjing Normal University supervision of Prof. Ya-Qian Lan. His research interest is related to the preparation of MOF materials for efficient electrocatalysis and photocatalysis.

Ya-Qian Lan was born in 1978 in Jilin, P. R. China. He received his B.S. and Ph.D. degrees (2009) from Northeast Normal University under the supervision of Prof. Zhong-Min Su. In 2010, he joined Prof. Qiang Xu's group at National Institute of Advanced Industrial Science and Technology (AIST, Japan) as a JSPS postdoctoral fellow. Since 2012, he has been a Professor of Chemistry at Nanjing Normal University. His current research interests focus on the application of polyoxometalate-based composite materials in energy storage and conversion and porous metal-organic frameworks for applications in catalysis and proton conduction.